Supporting Information for

Synergistic Magnetic proximity and Ferroelectric Field Effect on 2*H*-VS_2 Monolayer by Ferromagnetic Termination of $BiFeO_3$(0001) Surface

Jian-Qing Dai,* Jin Yuan, and Cheng Ke
Faculty of Materials Science and Engineering, Kunming University of Science and Technology, Kunming 650093, P. R. China

*Corresponding author. Fax: +86 871 65107922.
E-mail address: djqkust@sina.com (J.-Q. Dai).
ORCID: 0000-0003-4352-0789 (Jian-Qing Dai)

1. The choice of Hubbard parameter

For BFO, the Hubbard parameter U_{eff} was often in the range of 3–6 eV in order to obtain results consistent with experiments.[1] Our previous articles[2,3] demonstrated that the ferroelectric polarization and *G*-type AFM properties in bulk BFO can be well described by U_{eff} = 2.5–3.5 eV and the bandgap is determined to be ~ 2.1 eV for U_{eff} = 3.5 eV. As regards the VX_2 monolayers, the Hubbard parameter was usually set to be 2–3 eV.[4,5,6,7] We use the upper value of U_{eff} for V 3*d* electrons because of the frequent underestimation of bandgap even for DFT+*U* approach. Furthermore, our relevant work[8] indicated that, in 1*T*-VSe_2 monolayer, the magnetic moment of V atom shows a nearly saturated value at U_{eff} = 3.0 eV.

2. Electronic and magnetic properties of free-standing 2*H*-VS2 monolayer

From the U_{eff}-dependence of energy difference $\Delta E_{1T\text{-}2H}$ between the 1*T* and 2*H* phase (Fig. S1a), we find that the 2*H* phase is energetically preferred as $U_{eff} \leq 3.3$ eV and $\Delta E_{1T\text{-}2H}$ reaches a maximum value of 85.4 meV/f.u. at U_{eff} = 2.0 eV. The U_{eff}-dependence of the ground structure of VS_2 monolayer is in agreement with previous theoretical results[9,10] though the critical U_{eff} shows a different value to some degree because of the different functional used in our present work. In the following results, the upper value of U_{eff} = 3 eV ($\Delta E_{1T\text{-}2H}$ = 40.4 meV/f.u.) is adopted in view of the fact that bandgap is often underestimated for common Hubbard parameter in the DFT+*U* approach. At U_{eff} = 3 eV, the lattice constant of 2*H*-VS_2 monolayer is calculated to be 3.161 Å (without vdW correction), which is well consistent with

previous theoretical results.[9,11,12]

For the 2*H*-VS_2, Fig. S1a also shows the calculated total magnetization per formula unit (M_{tot}) and the magnetic moments of the V atom (M_V). We find that M_{tot} saturates to a value of 1.00 μ_B at $U_{eff} \geq 1.0$ eV, while M_V displays almost a linear increase as the Hubbard parameter larger than this value. Although the magnetization is dominantly localized on V atoms, our results demonstrate there are also some antiparallel magnetic moments on the S atoms. This can be understood from the $3d^1$ electron configuration of V^{4+} ion and the spin polarization induced by *p*-*d* orbital hybridization between V and S.[10,13] Furthermore, the antiparallel magnetic moments on S atoms indicates the existence of superexchange coupling between nearest V spins through the V-S-V path, which has been regarded as an important mechanism for the FM ground state.[13] By employing the default Wigner-Seitz radii (1.217 Å for V and 1.164 Å for S) in the VASP package, the value of M_V and M_S in the pristine 2*H*-VS_2 is respectively 1.099 μ_B and -0.098 μ_B at $U_{eff} = 3$ eV. In the existence of 2% tensile strain, the calculated M_V and M_S is increased to 1.146 μ_B and -0.113 μ_B, respectively. As pointed by Ref. [13], by using specific spin partitioning method, M_{tot} can be divided into the contribution from individual V and S atoms with the relationship of $M_{tot} = M_V + 2M_S$.

In addition to the magnetic moments, the exchange integral *J* between nearest V 3*d* spins and the magnetic anisotropy energy (MAE) are also determined. As shown by Fig. S2 in the Supporting Information, we use a 3×3 supercell to determine the energy difference ΔE_{mag} between FM and a ferrimagnetic (FiM) structure. For the FM and FiM configuration, the magnetic energy should be expressed respectively by $E_{FM} = -6J$ and $E_{FiM} = 6J$ because of the six nearest-neighbors around the central V atom displaying the same magnetic moment and opposite spin orientation. Therefore, the exchange integral equals to $J = \Delta E_{mag}/12$. For the free-standing VS_2 monolayer without and with 2% strain, the value of *J* is determined to be 59.02meV and 51.60 meV, respectively. Due to the easy-plane MAE (0.10 meV and 0.08 meV per formula unit for vanishing and 2% strain, respectively), we can estimate the critical temperature T_c by the Berezinsky-Kosterlitz-Thouless (BKT) transition,[14] i.e., $T_c = 0.89J/k_B$. For 2*H*-VS_2 with zero and 2% strain, the value of T_c is ~606 K and ~530 K, respectively, which is larger than the calculated value of 292 K and 115 K.[10,12] As we know, the estimated T_c of vdW-2D magnets often shows relatively large dispersion in literature due to the sensitivity of exchange integral to the employed functional and the Hubbard parameter.[15]

Next, we plot in Fig. S1b the band structure of pristine 2*H*-VS_2 monolayer. The magnetic semiconductive feature is evident. Although there exists clearly valley characteristics in the spin-up channel at *K* point, the conduction band minimum is located near the *M* point in the

spin-down channel. In other words, the bottom of conduction band and top of valence band are characterized by opposite spin polarization. This behavior is called bipolar magnetic semiconductor in Ref. [9]. As for the 2*H*-VS_2 monolayer with 2% strain, we find that this bipolar behavior disappears due to the upward shift of spin-down bands near the *M* point (Fig. S3a). For the spin-up and spin-down states, the band gap is determined to be 0.80 and 0.96 eV, respectively. Our present results are in agreement with previous theoretical reports[7,9,10] by using different exchange-correlation functional. By performing orbital-resolved projections, we find that the valence and conduction bands of the spin-up channels near the Fermi energy are dominant by V 3*d* states, while the corresponding spin-down channels display much stronger weight of S 3*p* orbitals. In addition, we should point out that, the *K* and *M* point of the primitive-cell Brillouin zone is folded into Γ and *m* point of the √3×√3 supercell Brillouin zone (Inset of Fig. S3a). In Fig. S3b and S3c, we show the folded band structure of free-standing 2*H*-VS_2 with 2% strain along *m*-Γ-*m* direction in the √3×√3 supercell Brillouin zone.

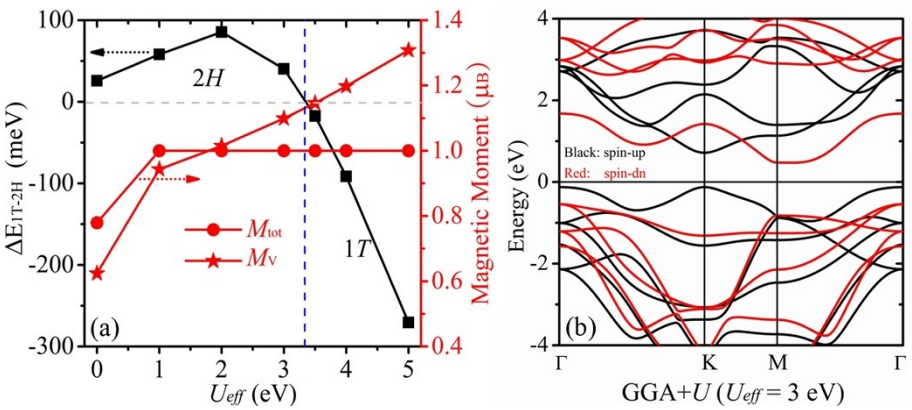

Fig. S1 (a) The U_{eff}-dependence of energy difference between 1*T* and 2*H* phase as well as magnetization of VS_2 monolayer and V atom (M_{tot} and M_V, respectively) in the 2*H*-phase. (b) Band structure of pristine 2*H*-VS_2 monolayer with U_{eff} = 3 eV. The black and red curves represent the spin-up and spin-down states, respectively. The energy scale is labeled relative to the Fermi level.

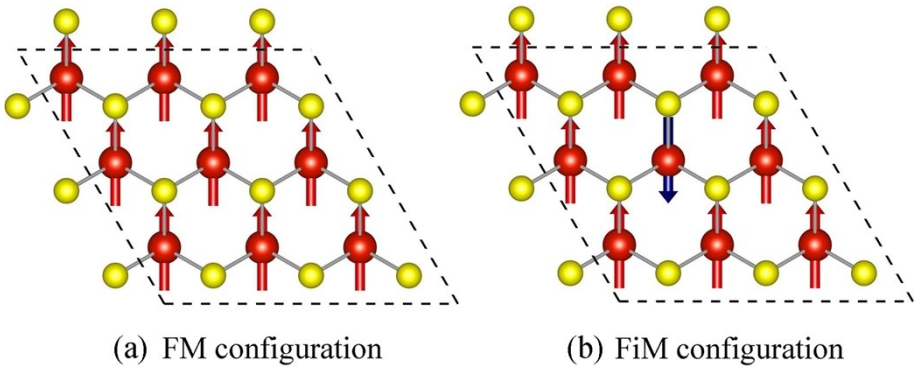

Fig. S2 (a) Ferromagnetic (FM) configuration and (b) ferrimagnetic (FiM) configuration in the 3×3 supercell of 2*H*-VS_2 monolayer for determining the exchange integral *J*.

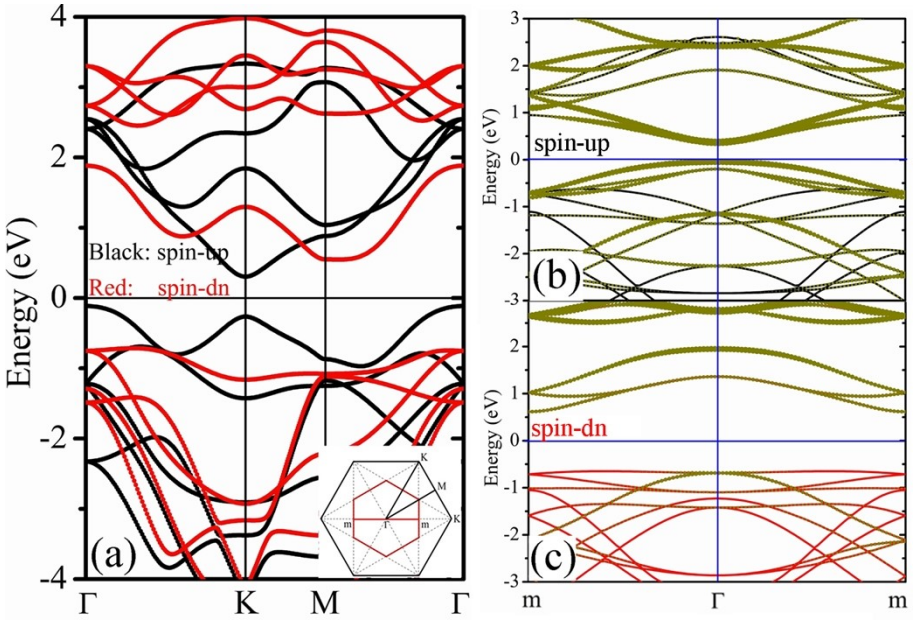

Fig. S3 (a) Band structure in primitive-cell Brillouin zone of free-standing 2*H*-VS_2 monolayer with 2.0% tensile strain. Inset shows the relationship of Brillouin zone between primitive-cell and √3×√3 supercell. The black and red curves indicate the spin-up and spin-down channels, respectively. (b) and (c) display respectively the spin-up and spin-down bands in the √3×√3 supercell Brillouin zone. The dark yellow circles represent the projection of V 3*d* orbitals and the size of the circles is proportional to the projection weight. The energy scale is labeled relative to the Fermi level.

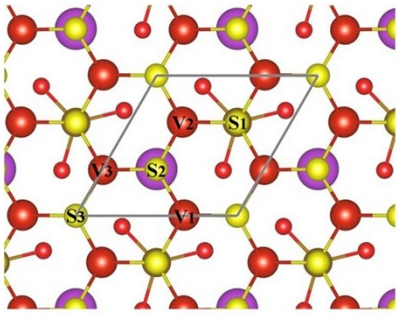

VS_2/N00	ΔQ (e)		M (μ_B)	
	PA	AP	PA	AP
V_1	-0.018	-0.017	1.288	1.185
V_2	-0.009	-0.010	1.282	1.193
V_3	-0.003	-0.004	1.227	1.140
S_1	-0.117	-0.129	-0.071	-0.105
S_2	-0.056	-0.048	-0.111	-0.106
S_3	0.027	0.033	-0.124	-0.121

(a) VS2/N00

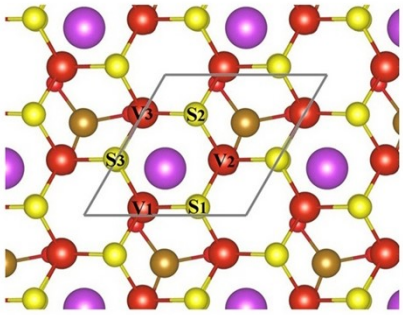

VS_2/N00′	ΔQ (e)		M (μ_B)	
	PA	AP	PA	AP
V_1	-0.027	-0.080	1.232	1.431
V_2	-0.025	-0.051	1.214	-1.250
V_3	-0.026	-0.051	1.218	-1.232
S_1	-0.134	-0.208	-0.088	0.001
S_2	-0.182	-0.236	-0.080	0.018
S_3	-0.178	-0.258	-0.080	0.013

(b) VS2/N00′

Fig. S4 Top-view of the 2*H*-VS_2/BFO(0001) heterostructure and the site-dependent atomic charge change (ΔQ) as well as atomic magnetic moment (M). (a) VS_2/N00 and (b) VS_2/N00′ hybrid system. For the top-view, in addition to the VS_2 monolayer, only the outmost -Bi-O_3-Fe trilayer of BFO(0001) substrate is included for clarity.

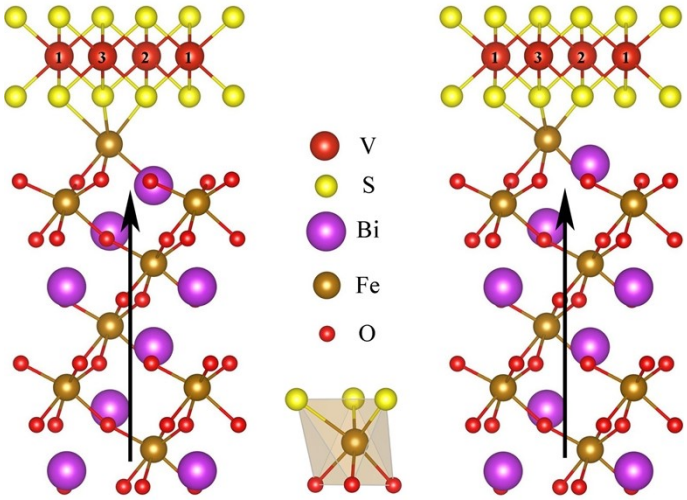

(a) VS2/N00′ PA (b) VS2/N00′ AP

Fig. S5 Side-view of the 2*H*-VS_2/N00′ hybrid structures with different magnetic proximity effect. (a) and (b) shows respectively the relaxed heterostructure with parallel (PA) and antiparallel (AP) interface magnetic configuration between the outmost Fe layer of BFO(0001) substrate and the 2*H*-VS_2 monolayer. The black arrow indicates the direction of ferroelectric polarization. The number shown on V denotes the site-resolved V atom illustrated in Fig. S3.

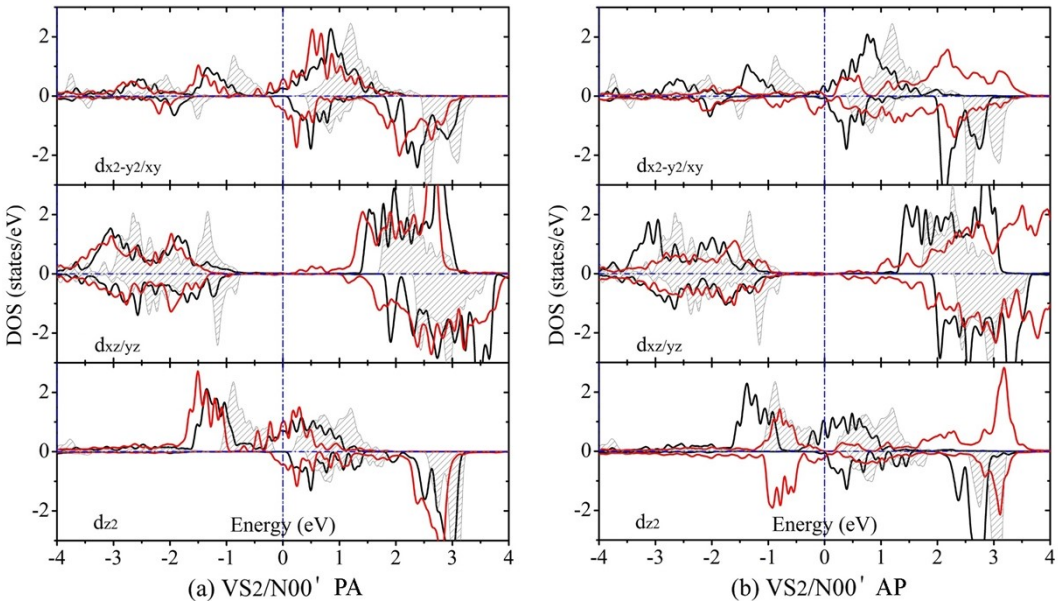

Fig. S6 Partial DOS of V-3*d* orbitals in the 2*H*-VS_2/BFO(0001) heterostructure. (a) PA interface magnetic configuration and (b) AP interface magnetic configuration. The black and red curves denote the partial DOS of VS_2/N00 and VS_2/N00′ system, respectively. To facilitate comparison, the partial DOS of free-standing 2*H*-VS_2 monolayer is also shown in the shadow area.

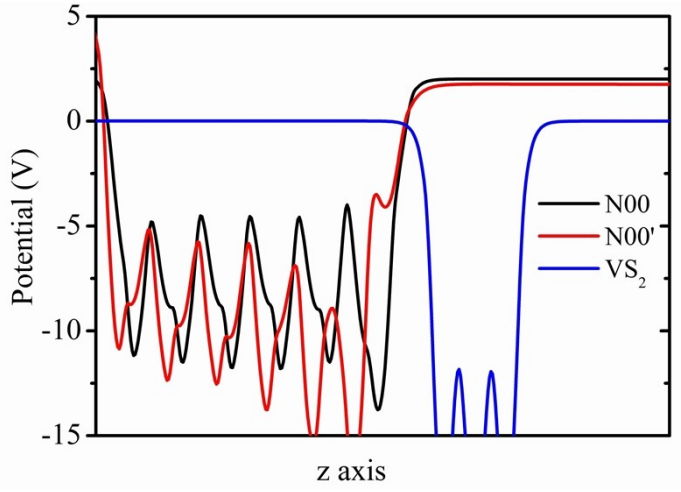

Fig. S7 Electrostatic potential distribution of the N00 and N00′ surfaces with respect to the free-standing 2*H*-VS_2 monolayer. The vacuum potential of 2*H*-VS_2 monolayer is set to zero point.

[1] S. Paul, D. Iuşan, P. Thunström, Y. O. Kvashnin, J. Hellsvik, M. Pereiro, A. Delin, R. Knut, D. Phuyal, A. Lindblad, et al. Investigation of the spectral properties and magnetism of $BiFeO_3$ by dynamical mean-field theory, Phys. Rev. B., 97 (2018) 125120.

[2] J.-Q. Dai, J.-W. Xu, and J.-H. Zhu, First-principles study on the multiferroic $BiFeO_3$ (0001) polar surfaces, Appl. Surf. Sci., 392 (2017) 135–143.

[3] J.-Q. Dai, J.-W. Xu, and J.-H. Zhu, Thermodynamic stability of $BiFeO_3$(0001) surfaces from *ab-initio* theory, ACS Appl. Mater. Interfaces, 9 (2017) 3168-3177.

[4] D. Dey and A. S. Botana, Structural, electronic, and magnetic properties of vanadium-based Janus dichalcogenide monolayers: a first-principles study, Phys. Rev. Mater., 4 (2020) 074002.

[5] M. Kan, B. Wang, Y. H. Lee, and Q. Sun, A density functional theory study of the tunable structure,

magnetism and metal-insulator phase transition in VS_2 monolayers induced by in-plane biaxial strain, Nano Res., 8 (2015) 1348–1356.

[6] H. L. Zhuang and R. G. Hennig, Stability and magnetism of strongly correlated single-layer VS_2, Phys. Rev. B, 93 (2016) 054429.

[7] Z. I. Popov, N. S. Mikhaleva, M. A. Visotin, A. A. Kuzubov, S. Entani, H. Naramoto, S. Sakai, P. B. Sorokinae, and P. V. Avramovd, The electronic structure and spin states of 2D graphene/VX_2 (X = S, Se) heterostructures, Phys. Chem. Chem. Phys., 18 (2016) 33047–33052.

[8] J.-Q. Dai, J. Yuan, C. Ke, and Z.-C. Wei, Tunable electronic and magnetic properties in 1T-VSe_2 monolayer on $BiFeO_3$(0001) ferroelectric substrate, Appl. Surf. Sci., 547 (2021) 149206.

[9] N. Luo, C. Si, and W. Duan, Structural and electronic phase transitions in ferromagnetic monolayer VS_2 induced by charge doping, Phys. Rev. B, 95 (2017) 205432.

[10] H. L. Zhuang and R. G. Hennig, Stability and magnetism of strongly correlated single-layer VS_2, Phys. Rev. B, 93 (2016) 054429.

[11] H.-R. Fuh, B. Yan, S.-C. Wu, C. Felser, and C.-R. Chang, Metal-insulator transition and the anomalous Hall effect in the layered magnetic materials VS_2 and VSe_2, New J. Phys., 18 (2016) 113038.

[12] H.-R. Fuh, C.-R. Chang, Y.-K. Wang, R. F. L. Evans, R. W. Chantrell, and H.-T. Jeng, Newtype single-layer magnetic semiconductor in transition-metal dichalcogenides VX_2 (X = S, Se and Te), Sci. Rep., 6 (2016) 32625.

[13] M. Aras and Ç. Kılıç, Magnetic ground state in $FeTe_2$, VS_2, and $NiTe_2$ monolayers: antiparallel magnetic moments at chalcogen atoms, Phys. Rev. B, 101 (2020) 054429.

[14] J. F. Fernández, M. F. Ferreira, and J. Stankiewicz, Critical behavior of the two-dimensional XY model: a Monte Carlo simulation, Phys. Rev. B, 34 (1986) 292.

[15] D. Torelli, K. S. Thygesen, and T. Olsen, High throughput computational screening for 2D ferromagnetic materials: the critical role of anisotropy and local correlations, 2D Mater., 6 (2019) 045018.